Optical and Electrical Properties of Er^{3+} Doped Glass

Magda Soares[1], Diogo Gomes[2], Ângelo Silva[3] e João Ribeiro[4]

[1]93348, mmfsoares@ua.pt, [2]93025, diogo.mf.gomes@ua.pt,
[3]100162, angelosilva@ua.pt, [4]109952, joao.pribeiro@ua.pt

Class P1

June 21, 2023

Abstract – In this work two glass samples were prepared by the melt-quenching method, one of them doped with 0.5% of Er_2O_3 compound, in order to analyze the effect of the presence of erbium ions in the physical, optical and electrical properties of the glass. With this objective, initially, the densities for both glasses, doped and undoped, were estimated, verifying that the density of the first one, (2.35 ± 0.04) g/cm^3, is higher than the second one, (2.27 ± 0.04) g/cm^3, as expected due to the higher molar mass of the Er_2O_3 compound, in relation to the others. In addition to this, it was found that the glass has 1.7×10^{20} Er^{3+} ions per cm^3. Next, the results obtained by double beam spectroscopy were analysed, verifying the presence of 11 absorption bands in the absorbance spectrum of the doped glass, due to the transitions from the $^4I_{15/2}$ ground state to various excited states of Er^{3+} ion, including two hypersensitive transitions at 521 nm ($^4I_{15/2} \rightarrow {}^2H_{11/2}$) and at 377 nm ($^4I_{15/2} \rightarrow {}^4G_{11/2}$). Additionally, using Tauc plot, the optical band gap energy for both direct ($E_{\text{gap}}^{\text{direct}}$) and indirect transitions ($E_{\text{gap}}^{\text{indirect}}$) was estimated. It was obtained $E_{\text{gap}}^{\text{direct}}$ equal to (3.901 ± 0.095) eV and (3.96 ± 0.23) eV, and $E_{\text{gap}}^{\text{indirect}}$ equal to (3.061 ± 0.038) eV and (3.156 ± 0.066) eV, for the undoped and doped glass, respectively. For the electrical properties were studied the electrical impedance, relative permittivity and the electric modulus for the doped glass in function of the frequency by impedance spectroscopy.

Key words – Dielectric properties, erbium, glass, UV-Vis absorption spectroscopy

1 Introduction

Glass has become an indispensable and essential component in fields such as optical communications, photovoltaic cells, home electronic equipment, vehicles, and building materials [1].

1.1 Structure and properties of glass

1.1.1 The vitreous state

Taking into account its structure, a glass can be defined as a non-crystalline solid exhibiting a glass transition. In fact, the atomic arrangement of glass lacks of a long range order as liquids; but, contrary to them, it is solid at room temperature. Besides, contrary to crystalline materials, there is neither crystal lattice nor lattice point in the structure of glass and thus, its X-ray diffraction (XRD) pattern presents a broad halo instead of the characteristic diffraction peaks of crystalline materials [2].

In the 1930s, Zachariasen introduced the random network theory on the atomic arrangement of glass. This theory considers that the structural units of glass and crystal are the same, but they are connected in different ways. For instance, the structural units that form the structure of amorphous silica (fused silica) and crystalline silica (quartz) are the same SiO_4 tetrahedra. But, they are randomly connected in fused silica, whereas they possess a periodic arrangement in quartz. However, the structure of glass exhibits a short range order (up to few Å), due to the chemical bonding constraints in local atomic polyhedra [2].

The most common glass network former is silica tetrahedron $(SiO_4)^{2-}$ connected with broad bond angle oxygen atom links to form a tetrahedral structure. Other glass formers are germanium oxide (GeO_2), boric oxide (B_2O_3), phosphorus pentoxide (P_2O_5), arsenic oxide (As_2O_3), phosphorus trioxide (P_2O_3), etc. These materials are capable of forming glass structure due to their low crystallisation rate and form three-dimensional matrices with oxygen atoms [3, 4].

In multi-component glasses, other compounds are added in a small percentage to modify the properties of the glass. They are called network modifiers, which includes the oxides of alkali-metals or alkali-earth metals. They participate in the glass network by occupying thermodynamic stable sites or by replacing some of the network formers [2, 3].

The increased number of large cations breaks bridges in the fundamental network, and the increased mobility of the building units and the modifiers easily account for the decreasing viscosity and melting range, as well as the increasing electrical conductivity of these conventional glasses [1]. In addition, Network modifiers can be used to facilitate the incorporation of trivalent rare earth ions [3].

Other compounds that may be part of the glass structure include the intermediate oxides, such as aluminium oxide, titanium oxide, and magnesium oxide. They are not able to form a glass on its own, taking part in the glass network only in the presence of a glass forming oxide [4].

The correlation between the chemical composition of glasses, their structure, and their macroscopic properties is on the basis of modern glass science [2].

1.1.2 Glass formation from melt and thermodynamic properties

Glass can be defined as a super-cooled liquid, which is in a thermodynamically metastable state. This definition is strictly related to the most common way to produce glass, that is through a fast cooling of a homogeneous melt obtained by melting high purity raw materials, consisting of a mixture of glass forming, modifier and/or intermediate oxides, at a high temperature [1, 2, 4].

This thermodynamic process can be described by considering the volume-temperature curve shown in figure 1. When a melt is cooled from a high temperature, its volume diminishes in a continuous way until it reaches the melting temperature T_m (line A-B). At this temperature, if the cooling rate is slower than the crystal growth rate, the melt goes through the region B-C and undergoes a contraction. Then further cooling of the melt can generate a solid crystalline material (line C-D). But, if the cooling rate is faster than the crystal growth rate, the melt passes Tm without crystallising and becomes a super-cooled liquid (line B-E). The transition between a super-cooled liquid to a solid glass (point E), which corresponds to a high value of viscosity, occurs at a temperature that is called the glass transition temperature, T_g. This temperature is not constant for a given glass but it depends on its cooling rate. In fact, a rapid cooling will produce a glass with a higher T_g and therefore, it will present a higher volume and a more open structure than a slowly cooled melt [2].

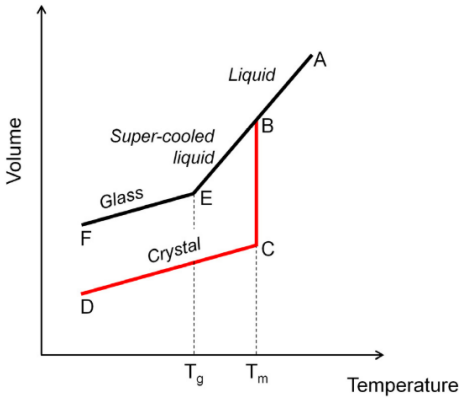

Figure 1: Volume-temperature curves for the formation of glass and crystal from a melt. Taken from [2].

1.2 Rare-earth Doped Glass

The versatility of rare-earth (RE) doped glasses in various optical applications has made them a subject of extensive research in glass science. These glasses find utility in solid-state laser materials, optical amplifiers, bar-code reading, three-dimensional displays, and remote sensing thermometers. Among the different RE ions, materials doped with Er^{3+} have garnered significant interest. When excited at 980 nm, these materials emit low energy infrared (IR) radiation at 1550 nm, making them crucial for telecommunication systems and optical amplifier devices [5].

1.2.1 Electronic and spectroscopic properties of rare-earth ions in a host material

The rare earths or lanthanides (Ln) elements possess electronic configuration $[\mathrm{Xe}]\,4f^n\,6s^2$ or $[\mathrm{Xe}]\,4f^{n-1}\,5d\,6s^2$, where [Xe] stands for the Xenon electronic structure, which includes the $5s$ and $5p$ electrons. When Ln elements are dispersed in a host matrix, they may attain either +2, +3 or +4 oxidation states, with +3 oxidation state being the most common. When a trivalent ion (Ln^{3+}) is formed, the atom gives up its outermost $6s$ electron, besides losing its $5d$ electron, if it has one. If it doesn't have, it loses one of the $4f$ electrons, leaving a partially filled $4f$ shell, shielded by the outer $5s$ and $5p$ shells. Depending on the number of $4f$ electrons, these can be distributed in different energy levels, which basically arise from electron-electron and electron-host interactions [6, 7].

Adopting the Russell-Saunders (LS) coupling scheme to label these energy levels, each energy level that can be occupied by $4f$ electrons in Ln^{3+} ions is denoted as $^{2S+1}L_J$, where: S is the total spin angular momentum; L is the total orbital angular momentum; and $J = S+L$ is the total angular momentum. L and S are the vector sums of the orbital and spin quantum numbers for all the $4f$ electrons of a given Ln^{3+} ion, respectively [2].

The splitting into several energy levels of a single $4f$ level results from several interactions. First, Coulomb, or electrostatic, interactions between $4f$ electrons lift the angular degeneracy and produce the ^{2S+1}L energy levels (LS terms), separated by an energy of $\sim 10^4$ cm^{-1}. Then, the spin-orbit coupling, the strongest of magnetic interactions, lifts the degeneracy in the total angular momentum (J) and splits the LS terms into J levels ($^{2S+1}L_J$), separated by $\sim 10^3$ cm^{-1}. The J levels represent the energy levels of a Ln^{3+} free ion. However, when the ion is in a host, electron-host interactions further split the J levels into to a maximum of $(J+1/2)$ Stark sublevels, due to the effect of the electric field that originates in a crystalline or glass host (crystal field effect). This effect is quite small (shifts the J levels only few $\sim 10-100$ cm^{-1}) compared to the previous ones since the $4f$ orbitals are shielded from the environment by the filled $5s$ and $5p$ sub-shells . This is an important characteristic in the spectroscopy properties of rare earth ions, since they maintain an atomic-like energy level structure even when they are incorporated in a host material [2, 7].

Nevertheless, the crystal field induced by the host is what determines the shape of the absorption and emission spectra of Ln^{3+} ions. The most relevant spectroscopic difference is observed when comparing the spectra of RE ions in crystals and glasses. In the first case, the absorption and emission bands have a very narrow bandwidth, even at room temperature. On the contrary, the spectra of RE ions in glasses show a broad bandwidth at room temperature. Two processes are responsible for the spectral broadening of Ln^{3+} ions in noncrystalline solids. The first is caused by lifetime broadening due to phonon-induced transitions among Stark components of the same J level. Since

this process is the same for each Ln^{3+} ion in the host, it is referred as homogeneous broadening. Instead, the second process results from the differences in the sites occupied by Ln^{3+} ions in the host, and thus, each Ln^{3+} experiences a different crystal field. In this case the process is termed inhomogeneous and the spectral broadening is the result of the energy distribution of each Stark sublevel [2].

Therefore, the spectral shape of the optical transitions of lanthanides in glasses is determined mostly by: Stark splitting of the degenerated energy levels of the free ion, determining the number of Stark level; magnitude of the splitting, which is determined by the host material; and different line broadening mechanisms, such as homogeneous and inhomogeneous broadening [8].

Transitions

According to Laporte's parity selection rule, electric dipole (ED) f-f transitions should be forbidden in Ln^{3+} ions since they are between states with the same parity. However, they become partially allowed when the Ln^{3+} ion is under the influence of a ligand field, because the interaction of the crystal field leads to the mix electronic states of opposite parity into the $4f$ wavefunctions, thus relaxing Laporte's selection rule. Apart from ED transitions, other types of f-f transitions are possible in Ln^{3+} ions. They are: magnetic dipole (MD) and electric quadrupole (EQ) transitions, that are parity allowed. However, the low symmetry of sites occupied by Ln^{3+} ions in glasses makes MD and EQ transitions weaker than ED transitions [2] .

Since the electric dipole transitions are weakly allowed, they present low absorption coefficients and relatively long lifetimes (up to several milliseconds). Though the shielding of the $4f$ electrons by the s and p shells makes them almost insensitive to the near field, a few transitions exaggerate the small changes in the lattice coordination sphere. These transitions are termed hypersensitive transitions. Their intensity is significantly enhanced as the symmetry of the Ln complex lowers or the polarizability of the ligands increases. Jørgenson and Judd noted that hypersensitive transitions obey the selection rules $\Delta J \geq 2, \Delta L \geq 2, \Delta S \geq 0$ [6].

1.2.2 Spectroscopic of Erbium

Erbium (Er) is a rare earth element, with electronic configuration of the neutral free Er atoms being $[\mathrm{Xe}]\, 4f^{12}\, 6s^2$. The trivalent charge state of erbium (Er^{3+}) occurs by losing two electrons and one electron from, respectively, the $6s$ and the $4f$ shells. Therefore, the electronic configuration of Er^{3+} ions consists of a Xe core and comprises of 11 $4f$-electrons [7].

In agreement with the explanation given earlier, the electrons in the incomplete $4f$-shell are effectively screened by the two complete remaining shells with larger radial extensions, the $5s^2$ and the $5p^6$ shells, and so the effect of the host field is limited, changing slightly the relative position of the energy levels of Er^{3+} and perturbing the wave functions of $4f$-electrons [7].

The energy distribution of the $4f^{11}$ levels originates from electron-electron and spin-orbit interactions. Those atomic interactions split the original $4f^{11}$ configuration of one electron orbital into $^{2S+1}L_J$ levels. Furthermore, as the result of the asymmetric distribution of charge density surrounding the Er^{3+} ion caused by the host field, the degeneracy of the $4f$ atomic spin-orbit coupling states is lifted, giving rise to a maximum number of $J + 1/2$ Stark sates. So, there are at most 8 states for the ground energy level ($J = 15/2$) and 7 states for the first-excited energy level ($J = 13/2$), which may be altered from homogeneous and/or inhomogeneous broadening [7].

Figure 2 shows the energy level diagram for Er^{3+} (free ion). With the advent of fibre optic communications, erbium has been of extensive interest because of its emission around 1550 nm (due to $^4I_{13/2} \rightarrow {}^4I_{15/2}$ transition) corresponding to the third telecommunications transmission window. Erbium-doped fibres (EDFs) have brought about a revolution in communications systems with its use as amplifiers, repeaters and fibre lasers [3, 9].

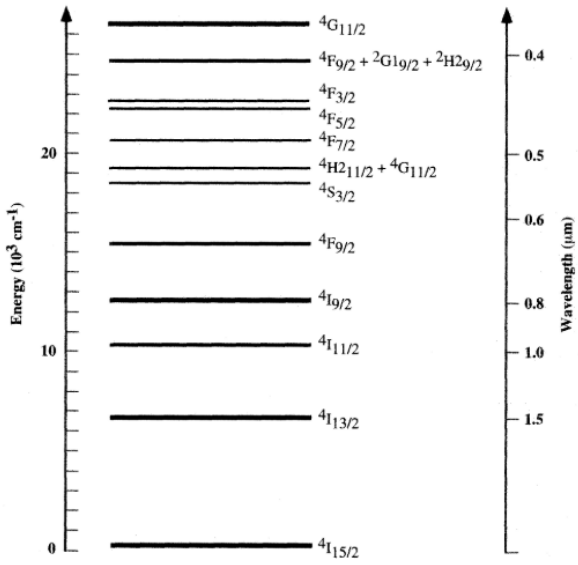

Figure 2: Energy level structure of Er^{3+}. The wavelength scale corresponds to the wavelength of the transition from a given energy level to the ground state [9].

2 Experimental Procedure

2.1 Glass Preparation

In this work the glasses studied were produced by the melt-quenching technique. In fact, the vast majority of the glasses are produced by this method [10]. A schematic representation of glass preparation by the melt-quenching technique is depicted in figure 3.

The raw materials used for the production of the glasses are listed in table 1, as well as their molar percentages. The reagent powders were weighed (to a total of 10 g) according to the stoichiometric compositions of

the compounds. Using (1) and (2) it was possible to determine the number of moles of the compound and the mass of each reactant.

$$n = \frac{m}{M} \tag{1}$$

$$\text{mol}(\%) = \frac{n_{reagent}}{n_{compound}} \times 100 \tag{2}$$

where n is the number of moles, m is the mass and M is the molar mass.

Table 1: Composition of the studied glasses.

Compounds	Undoped glass (mol%)	Doped glass (mol%)
B_2O_3	50	49.5
Na_2CO_3	35	35
SiO_2	10	10
Al_2O_3	5	5
Er_2O_3	-	0.5

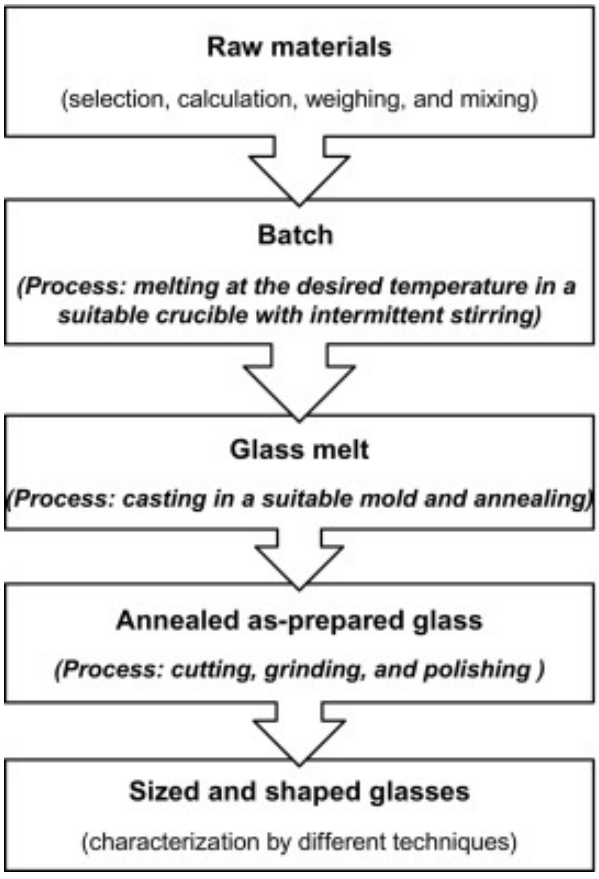

Figure 3: Schematic illustration of different steps of glass preparation by the melt-quenching technique [10].

Firstly, the starting materials were mixed thoroughly by grinding in an ceramic mortar. Subsequentely the powders were placed in an alumina crucible which in turn was placed in the furnace for the fusion process at a temperature of 1000 °C. The melted mixture was then poured onto a heated brass plate at 300 °C (this process is called quenching). The glass was subjected to an annealing process to relieve glass internal stresses, in which it was baked for twelve hours at a temperature of 300 °C. Finally, the sample was cooled down to room temperature. This procedure was repeated for doped and undoped glass. The rare earth compound used for the doped glass was Er_2O_3.

The glass samples thus prepared were polished until a flat surface was achieved, with different grids of SiC abrasive discs for further optical characterizations. The equipment used can be seen in the figure 4.

Figure 4: Polishing machine used to polish glasses in the laboratory.

2.2 Physical, Optical, Electrical properties and instrumentation details

After the preparation of the glasses, their properties were characterised. Firstly, some physical properties were studied. Due to the shape of the glasses it was assumed that the best approximation would be to consider the glass as a cylinder, thus measuring the radius and height (thickness). These measurements were made with a pachymeter. In order to calculate the density of the glasses, their masses were measured with a digital balance.

For the characterization of the optical properties the UV-Vis absorption technique was used with the aid of a double beam spectrophotometer *Shimadzu UV-2100*. In the sample position the glass was placed attached to the support with adhesive paste while in the reference position nothing was placed in the support (air). The instrumental parameters used during the measurements are given by the table 2.

Table 2: Spectrum and instrumental parameters.

Measuring Mode	Abs
Recording Range	0-1
Wavelength Range (nm)	200-900
Scan Speed	Medium
Slit Width (nm)	2.0
Sampling interval (nm)	0.5
Light Source Change Wavelength	360
Detector Change Wavelength	830
S/R Exchange	Normal
Detector Lock	PM

Finally for the characterization of the electrical properties, it was required to apply a thin layer of silver paint on the surfaces of the glasses without passing the edges in order to make the electrical contacts. When the ink was dry the samples were connected to a four terminals LCR Meter *BK PRECISION TL89K1.* A different doped glass sample than the physical properties was used for these measurements. The equivalent circuit used in the equipment for the impedance spectroscopy was the circuit paralell RC. The values of C and R were obtained for a frequency sweep between 1.177 kHz and 300 kHz. The experimental parameters are shown in table 3.

Table 3: Experimental parameters of the measurements with the LCR Meter.

Start Frequency	1.177 kHz
Stop Frequency	300.0 kHz
Level	0.5 VRMS
Step	10
Autoscale	ON
Scale	LINEAR

3 Results and Discussion

3.1 Physical Properties

Table 4 shows the results of the measurements of the physical properties mentioned in subsection 2.2

Table 4: Measurement of the physical properties of glasses.

	Undoped glass	Doped glass
Thickness (mm)	3.44 ± 0.02	4.00 ± 0.02
Diameter (mm)	14.84 ± 0.02	11.64 ± 0.02
Mass (g)	1.35 ± 0.01	1.00 ± 0.01

Considering glasses with a cylindrical shape as mentioned in subsection 2.2, their volume can be calculated by the following equation:

$$V = \pi \frac{d^2}{4} t \tag{3}$$

where d is the diameter and t the thickness. The associated error is given by the errors propagation method:

$$\Delta V = \left|\frac{\partial V}{\partial d}\right| \Delta d + \left|\frac{\partial V}{\partial t}\right| \Delta t = \frac{\pi d t}{2} \Delta d + \frac{\pi d^2}{4} \Delta t \tag{4}$$

Through (3) and (4) and with the information given in table 4 the volume of the two glasses was calculated, obtaining (0.425±0.004) cm^3 for the doped glass and (0.595±0.005) cm^3 for the undoped one. The density of glasses can be calculated using the following equation:

$$\rho = \frac{m}{V} \tag{5}$$

where the associated error is given by:

$$\Delta \rho = \left|\frac{\partial \rho}{\partial V}\right| \Delta V + \left|\frac{\partial \rho}{\partial m}\right| \Delta m = \frac{1}{V} \Delta m + \frac{m}{V^2} \Delta V \tag{6}$$

Thus the densities of (2.35±0.04) g/cm^3 for the doped glass and (2.27±0.04) g/cm^3 for the undoped glass were obtained. Finally, it was intended to determine the concentration of Er^{3+} dopant ions. The concentration of an RE (rare-earth) dopant in a glass can be estimated by [11]:

$$C[\text{ions/cm}^3] = \frac{w_{RE} \times \rho_{doped} \times N_A \times N_{RE}}{w_{glass} \times M_{compound}} \tag{7}$$

where w_{RE} is the weight of RE ion compound, ρ_{doped} the density of doped glass, N_A the Avogadro's number (6,022 × 10^{23} atoms/mol), N_{RE} the number of RE atoms in RE compound, w_{glass} the total weight of glass (10 g) and $M_{compound}$ the molecular weight of RE compound.

As previously mentioned, the rare earth compound used as dopant was Er_2O_3, where we have two rare-earth ion Er^{3+}. The molecular weight of Er_2O_3 is 382.56 g/mol and the weight of Er_2O_3 utilized was 0.226 g. Using these values and those previously calculated, the concentration of the dopant ion Er^{3+} in the doped glass obtained was 1.7 × 10^{20} ions/cm^3.

By analysing the density of the two glasses it can be seen that the insertion of erbium ions increases the density of the sample. This is explained by the higher molecular weight of Er_2O_3 (382.56 g/mol) in relation to B_2O_3 (69.62 g/mol), Na_2CO_3 (105.99 g/mol), SiO_2 (60.08 g/mol) and Al_2O_3 (101.96 g/mol) [12].

It must be taken into account that the method used to calculate the density of glass has its limitations. Evidently, considering the shape of the glass as a cylinder for the volume calculation will lead to the result obtained being significantly different from the real one, since the shape of the glass does not perfectly correspond to a cylinder. In the literature [13] it is typically mentioned the Archimedes method for measuring the density of glass. Typically for small glass samples heavy liquids are used. In [11] the densities of the prepared glasses were determined employing Archimedes principle in which glass was weighed in air and then in xylene liquid at room temperature using a balance. The density (ρ) was calculated using the formula:

$$\rho = \frac{W - W_1}{W} \times 0.865 \tag{8}$$

where W is the weight of the prepared glass sample in air, W_1 the weight of the prepared glass sample in xylene and 0.865 the density of xylene at room temperature.

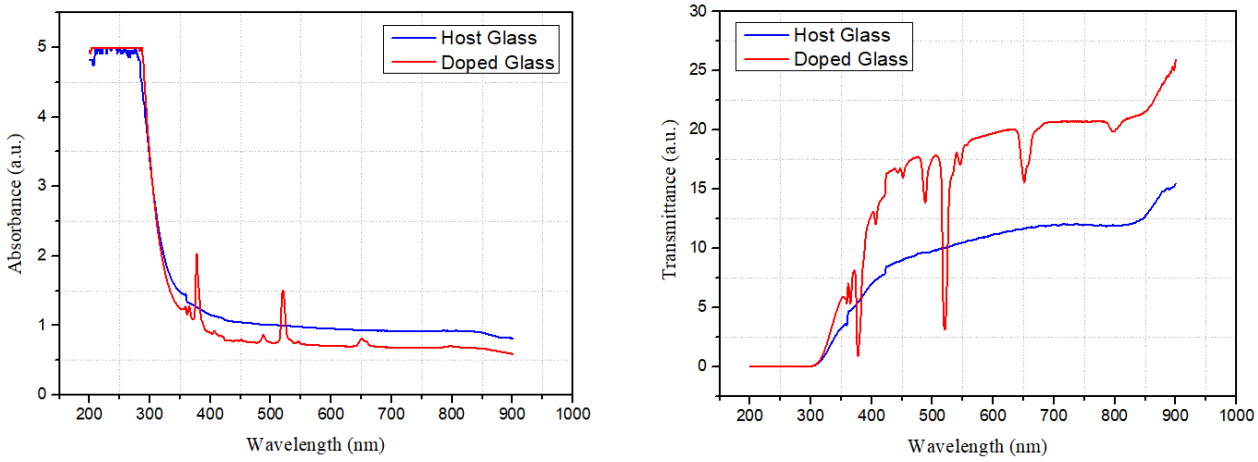

(a) (b)

Figure 5: Host and doped glass absorbance (a) and transmittance (b) spectra.

3.2 Optical Properties

The absorption and transmittance spectra of the host glass and erbium doped glass samples are shown in Figure 5. Comparing both absorption spectra, the doped glass exhibits a much higher number of absorption bands, resulting from the optical properties of rare earth ions.

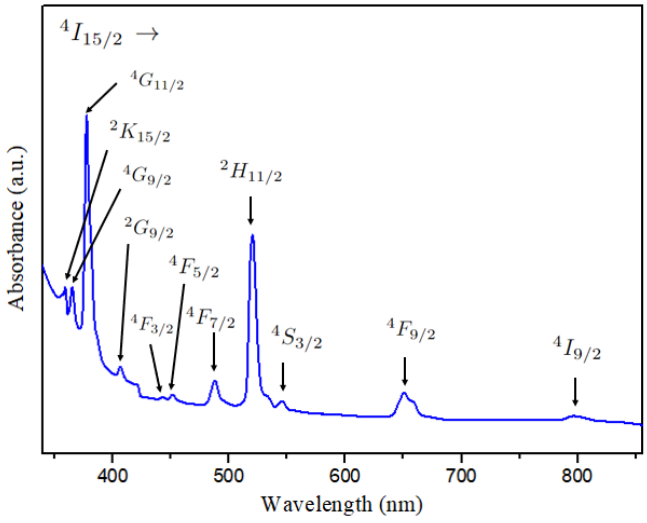

Figure 6: The absorption spectra of the doped glass, showing the absorption bands due to the transitions from the $^4I_{15/2}$ ground state to various excited states of Er^{3+} ion.

Figure 6 shows the optical absorption spectrum of the Er^{3+} doped glass in the range 340-850 nm. The absorption bands observed for the doped sample occurs due to 4f–4f electric dipole transitions from the $^4I_{15/2}$ ground state to various excited states of Er^{3+} ions. The absorption spectrum consists of 11 absorption bands at wavelengths 359 nm, 365 nm, 377 nm, 406 nm, 442 nm, 451 nm, 488 nm, 521 nm, 545 nm, 650 nm and 796 nm corresponding to the transitions (from $^4I_{15/2}$ →) to $^2K_{15/2}$, $^4G_{9/2}$, $^4G_{11/2}$, $^2G_{9/2}$, $^4F_{3/2}$, $^4F_{5/2}$, $^4F_{7/2}$, $^2H_{11/2}$, $^4S_{3/2}$, $^4F_{9/2}$ and $^4I_{9/2}$, respectively. Among all these transitions, the transitions $^4I_{15/2} \rightarrow {}^2H_{11/2}$ (521 nm) and $^4I_{15/2} \rightarrow {}^4G_{11/2}$ (377 nm) are named as hpersensitive transitions. The intensities of these hypersensitive transitions are very sensitive to small changes of the glass environment throughout the rare-earth ions. The electronic transitions observed in the spectrum were identified based on the literature [14, 15, 16, 17], where other types of Er^{3+} doped glasses are the subject of study.

Optical band gap energy

The energy difference between the valence band and the conduction band is known as the band gap energy. We can determine the optical gap values for the present glasses using Tauc plot, which establishes the relation between optical band gap energy (E_{gap}) and optical absorption coefficient of glasses (α) as follows:

$$\alpha\,(h\nu) \propto (h\nu - E_{\text{gap}})^n, \tag{9}$$

where $h\nu$ refers to photon energy and n is an index number related to characteristic band gap transition with $n = 1/2$ for direct allowed transition and $n = 2$ for indirect allowed transition [14, 18, 19]. Using equation 9, optical band gap of glasses can be estimated by extrapolating the linear part of the curve to the horizontal axis ($h\nu$) from the plot of $[\alpha(h\nu)^2]$ vs. $h\nu$ for direct optical band gap and $[\alpha(h\nu)^{1/2}]$ vs. $h\nu$ to determine indirect optical band gap of the glasses.

Using Beer-Lambert law, we can determine the absorption coefficient using the equation $\alpha = \ln(1/T)/t$, where t is the thickness and T the transmittance of the sample. The absorbance A is defined as $A = \log(1/T)$. So changing the base of the logarithm, we obtained $\alpha = 2,303A/t$.

Tauc plots for the direct and indirect optical band gap can be observed in figures 7 and 8 for the undoped and doped glass, respectively. The results obtained are shown in table 5. Analysing them, it can be seen that with doping there is an increase in the band gap, for both direct and indirect transitions, which is in disagreement

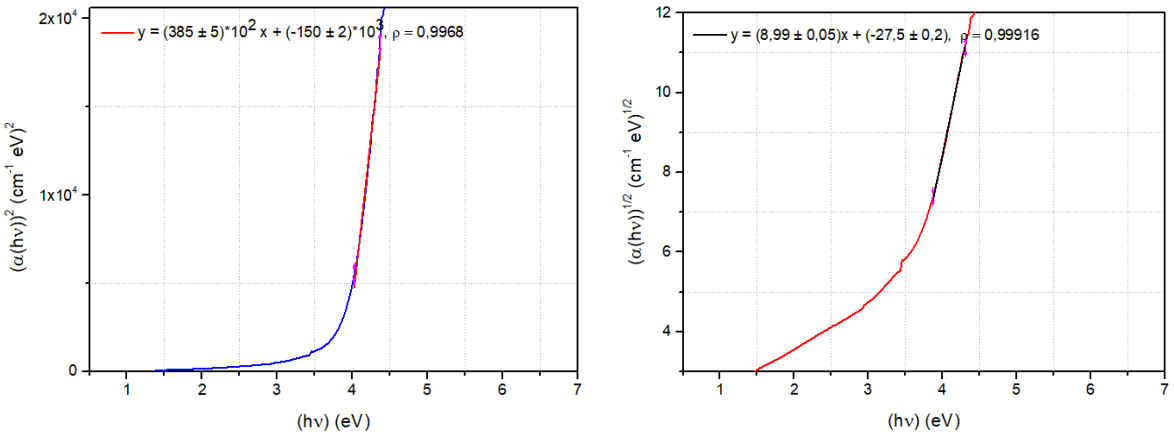

(a) (b)

Figure 7: Tauc's plot $[\alpha(h\nu)^2]$, $[\alpha(h\nu)^{1/2}]$ as a function of photon energy $(h\nu)$ for direct (a) and indirect (b) allowed transitions of undoped glass. The E_{gap} values were obtained by extrapolating the linear region of the curve to $(\alpha\,(h\nu))^{1/n} = 0$.

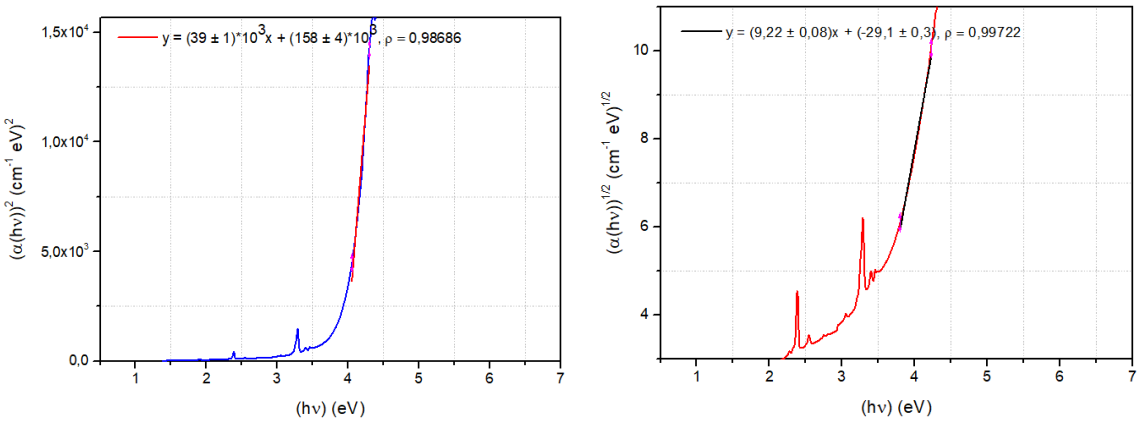

(a) (b)

Figure 8: Tauc's plot $[\alpha(h\nu)^2]$, $[\alpha(h\nu)^{1/2}]$ as a function of photon energy $(h\nu)$ for direct (a) and indirect (b) allowed transitions of doped glass. The E_{gap} values were obtained by extrapolating the linear region of the curve to $(\alpha\,(h\nu))^{1/n} = 0$.

with the behaviour observed in the study of other Er^{3+} doped glasses [14, 20]. The band gap energy is influenced not only by the chemical composition but also by the structural arrangement of the chosen host matrix, so that a further direct comparison with the values reported in studies of different erbium doped glasses is not adequate.

Table 5: Direct and indirect optical band gaps for the undoped and doped glass samples.

Glass	$E_{\text{gap}}^{\text{direct}}$	$E_{\text{gap}}^{\text{indirect}}$
Undoped	$3,901 \pm 0,095$	$3,061 \pm 0,038$
Doped	$3,96 \pm 0,23$	$3,156 \pm 0,066$

For last, the graph of absorption cross-section (σ) as a function of wavelength was made for the doped glass (see figure 9), using the following definition: $\sigma = A\,/\,N\,t$, where A is the absorbance, N is the rare earth ion concentration per unit volume and t is the thickness of the sample [2].

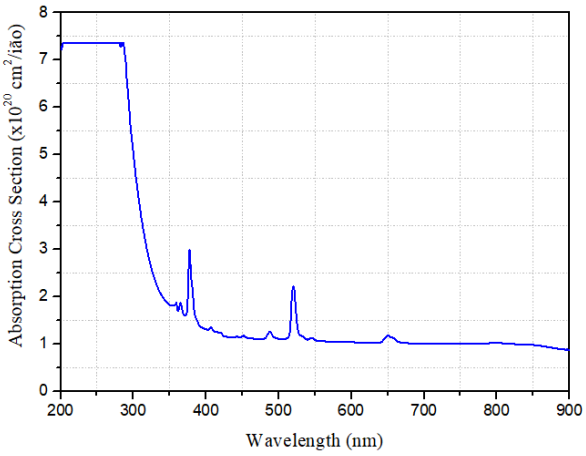

Figure 9: Absorption cross-section for the erbium doped glass.

3.3 Electrical Properties

Figure 10 and figure 11 show the behaviour of resistance and capacitance of doped glass as a function of frequency. The doped glass used in this electrical characterization had a thickness of (3.14 ± 0.02) mm and a diameter of (11.50 ± 0.02) mm. It should be noted that, although data were taken for frequencies up to 300 kHz, for values above 9.189 kHz negative capacitance values were obtained, indicating that the LCR could not make accurate measurements for that frequency range.

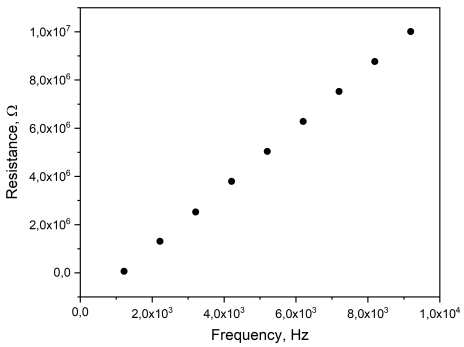

Figure 10: Resistance versus frequency.

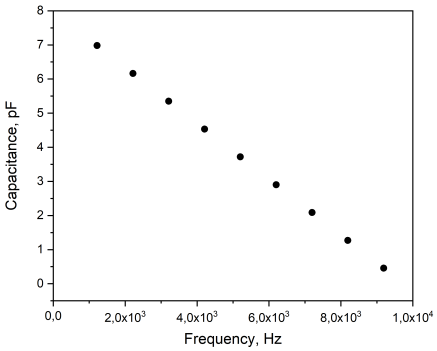

Figure 11: Capacitance versus frequency.

Based on these results the electrical impedance, relative permittivity and electric modulus were analysed. The complex value of the dielectric constant is given by:

$$\epsilon^* = \epsilon' - i\epsilon'' \tag{10}$$

Where ϵ' is the real part of relative permittivity and ϵ'' is the imaginary part. The real and imaginary part are given by:

$$\epsilon' = \frac{Cd}{\epsilon_0 A} \tag{11}$$

$$\epsilon'' = \frac{d}{\epsilon_0 A w R} \tag{12}$$

Where C and R represent the measured capacitance and resistance, d the sample thickness, A the electrode area, w the angular frequency and ϵ_0 the vacuum permittivity.

With these two components calculated, the modulus of the dielectric constant can be calculated by:

$$\epsilon = \sqrt{\epsilon'^2 + \epsilon''^2} \tag{13}$$

The results concerning the relative permittivity can be seen in the figures 12,13,14 and 15.

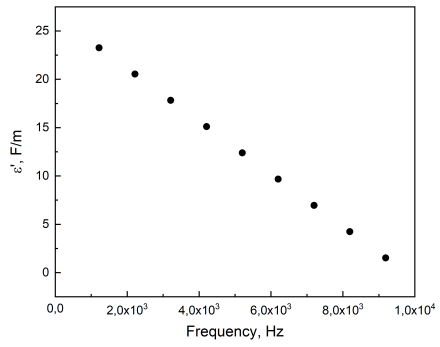

Figure 12: Real part of the dielectric constant versus frequency.

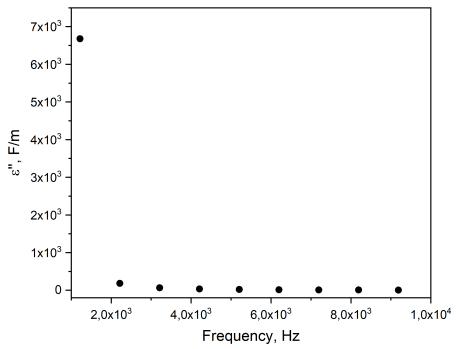

Figure 13: Imaginary part of the dielectric constant vs frequency.

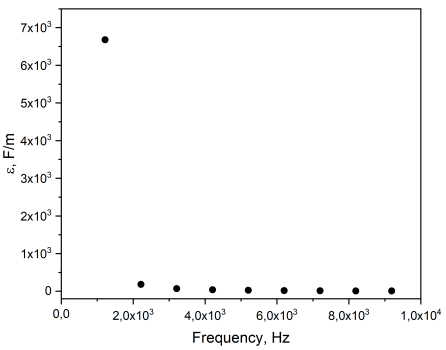

Figure 14: Dielectric constant modulus versus frequency.

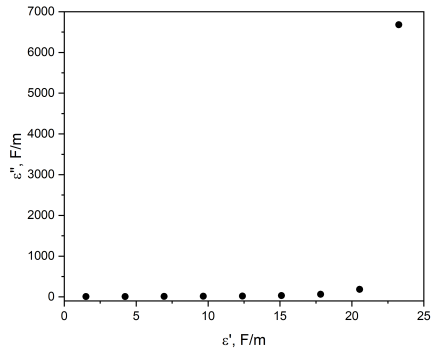

Figure 15: Imaginary part of the dielectric constant versus the real part of the dielectric constant.

Electrical impedance is also divided into a real and imaginary part. Its real, imaginary parts and modulus being given by:

$$Z' = \frac{\epsilon''}{2\pi f C_0(\epsilon'^2 + \epsilon''^2)} \tag{14}$$

$$Z'' = \frac{\epsilon'}{2\pi f C_0(\epsilon'^2 + \epsilon''^2)} \tag{15}$$

$$Z = \sqrt{Z'^2 + Z''^2} \tag{16}$$

Where $C_0 = \epsilon_0/At$ and f is the frequency. The results are shown in figures 16 and 17.

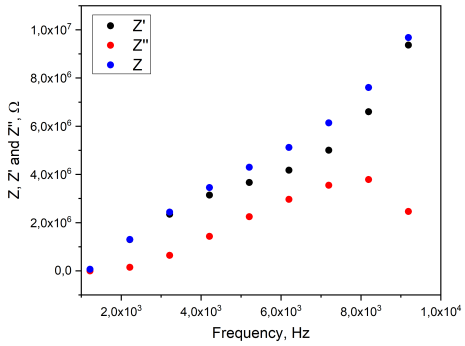

Figure 16: Real part, imaginary part and modulus of the electrical impedance versus frequency.

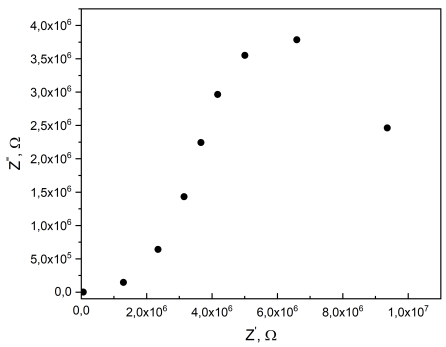

Figure 17: Nyquist plot.

The electric modulus can be divided into a real part and an imaginary part. These components and the absolute value are given by:

$$M' = \frac{\epsilon''}{\epsilon''^2 + \epsilon'^2} \tag{17}$$

$$M'' = \frac{-\epsilon''}{\epsilon''^2 + \epsilon'^2} \tag{18}$$

$$M = \sqrt{M'^2 + M''^2} \tag{19}$$

The results concerning the behaviour of the electric module can be observed in the figures 18 and 19.

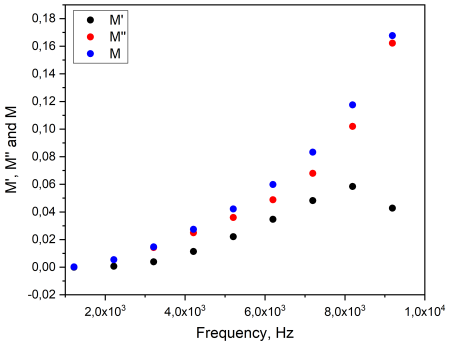

Figure 18: Real part, imaginary part and the absolute of the electric modulus versus frequency.

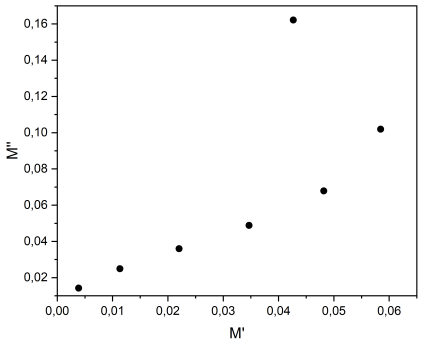

Figure 19: M" versus M'.

Analysing the figures 10 and 11 it is possible to see a linear behaviour of resistance and capacitance with increasing frequency. Resistance increased with frequency, while capacitance decreased. The real part of the relative permittivity (figure 12) also shows a decreasing linear behaviour with increasing frequency. The real part of the relative permittivity is a measure of how much energy from an external electric field is stored in a material, representing the amount of dipole alignment in a given volume. This way, we can conclude that the glass with the increase of frequency begins to lose the capacity to store charge. By means of the figure 13 we can observe a drastic decrease in the value of the imaginary part of the dielectric constant to 2.217 kHz stabilizing to values below 100 F/m for higher frequencies. The decrease of

the imaginary permittivity indicates lower losses of the glass for higher frequencies. This factor includes the effects of both dielectric loss and conductivity.

The impedance plots (figures 16 and 17) indicate a high dependence of the absolute value of the impedance on the imaginary part for all frequencies. The nyquist plot has its origin at 0 indicating that the equivalent circuit of the glass should have no series resistances. It is complicated to draw a clear conclusion from the Nyquist plot, due to the fact that we have few points, however it is observed a behaviour that is relatively close to a circle, which may indicate that the equivalent circuit of the resistor in parallel with the capacitor is a good approximation. In the frequency range studied, no peaks were observed in the plot of the imaginary part of the electric modulus. These peaks are typically reported in the literature due to dielectric relaxation processes [21].

4 Conclusion

The main objectives of this work were accomplished. Two glass samples, one doped with 0.5% of Er_2O_3 compound, were prepared by the melt-quenching method, and characterized by their optical and electrical properties. In addition, some physical properties were studied, including the densities of both glasses and the concentration of erbium ions on the doped glass sample. A higher density was obtained for the doped glass (2.35 $\pm$ 0.04) g/cm^3 compared to the undoped one (2.27 $\pm$ 0.04) g/cm^3, which is expected due to the high molecular weight of Er_2O_3 relative to the other glass compounds. However due to the method used to obtain the density these results may not be translated into the real ones being suggested to use the Archimedes method with liquid xylene for a better accuracy.

With respect to the optical characterization, 11 absorption bands were observed for the doped sample as a result of 4f–4f electric dipole transitions from the $^4I_{15/2}$ ground state to various excited states of Er^{3+} ions: $^2K_{15/2}$, $^4G_{9/2}$, $^4G_{11/2}$, $^2G_{9/2}$, $^4F_{3/2}$, $^4F_{5/2}$, $^4F_{7/2}$, $^2H_{11/2}$, $^4S_{3/2}$, $^4F_{9/2}$ and $^4I_{9/2}$, at wavelengths 359 nm, 365 nm, 377 nm, 406 nm, 442 nm, 451 nm, 488 nm, 521 nm, 545 nm, 650 nm and 796 nm, respectively, with $^4I_{15/2} \rightarrow {}^2H_{11/2}$ and $^4I_{15/2} \rightarrow {}^4G_{11/2}$ being hypersensitive transitions. Additionally, using Tauc method the optical band gap energy for both direct and indirect transitions was estimated, where we found that with doping there is an increase in the band gap, which is in disagreement with the behaviour reported in the study of other Er^{3+} doped glasses [14, 20].

From the electrical characterisation it was difficult to draw a clear conclusion from the Nyquist plot about the equivalent circuit and it is suggested to acquire data for more frequency values. However, everything indicates that the equivalent circuit model does not present series resistances. It was observed that with increasing frequency the glass presented less capacity to store charge. The dielectric losses decreased with increasing frequency.

References

[1] Z.-H. Jiang and Q.-Y. Zhang, "The structure of glass: a phase equilibrium diagram approach," *Progress in Materials Science*, vol. 61, pp. 144–215, 2014.

[2] R. Morea, *Synthesis and characterization of rare earth doped fluorotellurite glasses, glass-ceramics, and thin film glasses for active photonic applications*. PhD thesis, Facultad de Ciencias de la Universidad Autónoma de Madrid, 2015.

[3] N. Tamchek, *Characterisation of bismuth-based erbium-doped fibre and its application in wide-band optical amplifiers*. PhD thesis, University Malaya, 2009.

[4] A. S. Alzahrani, "A review of glass and crystallizations of glass-ceramics," *Advances in Materials Physics and Chemistry*, vol. 12, no. 11, pp. 261–288, 2022.

[5] D. Manzani, M. Montesso, C. Mathias, K. V. Krishanaiah, S. Ribeiro, and M. Nalin, "Visible up-conversion and near-infrared luminescence of er3+/yb3+ co-doped sbpo4-geo2 glasses," *Optical Materials*, vol. 57, pp. 71–78, 2016.

[6] Y. Dwivedi and S. C. Zilio, "Advances in rare earth spectroscopy and applications," *Journal of nanoscience and nanotechnology*, vol. 14, no. 2, pp. 1578–1596, 2014.

[7] S. Gallis, *Erbium-doped silicon-oxycarbide materials for advanced optical waveguide amplifiers*. PhD thesis, University at Albany, College of Nanoscale Science and Engineering, 2006.

[8] V. Ter-Mikirtychev, *Fundamentals of fiber lasers and fiber amplifiers*, vol. 99. Springer, 2014.

[9] P. M. Becker, A. A. Olsson, and J. R. Simpson, *Erbium-doped fiber amplifiers: fundamentals and technology*. Elsevier, 1999.

[10] B. Karmakar, "Chapter 1 - fundamentals of glass and glass nanocomposites," in *Glass Nanocomposites* (B. Karmakar, K. Rademann, and A. L. Stepanov, eds.), pp. 3–53, Boston: William Andrew Publishing, 2016.

[11] K. Annapoorani, C. Basavapoornima, N. Suriya Murthy, and K. Marimuthu, "Investigations on structural and luminescence behavior of er3+ doped lithium zinc borate glasses for lasers and optical amplifier applications," *Journal of Non-Crystalline Solids*, vol. 447, pp. 273–282, 2016.

[12] A. Martins, C. Feitosa, W. Santos, C. Jacinto, and C. Santos, "Influence of bax2 (x = cl, f) and er2o3 concentration on the physical and optical properties of barium borate glasses," *Physica B: Condensed Matter*, vol. 558, pp. 146–153, 2019.

[13] M. tang Wang, J. shu Cheng, M. Li, and F. He, "Structure and properties of soda lime silicate glass doped with rare earth," *Physica B: Condensed Matter*, vol. 406, no. 2, pp. 187–191, 2011.

[14] S. Taherunnisa, D. K. Reddy, T. SambasivaRao, K. Rudramamba, Y. Zhydachevskyy, A. Suchocki, M. Piasecki, and M. R. Reddy, "Effect of up-

conversion luminescence in Er^{3+} doped phosphate glasses for developing erbium-doped fibre amplifiers (edfa) and g-led's," *Optical Materials: X*, vol. 3, p. 100034, 2019.

[15] C. Basavapoornima, K. Linganna, C. Kesavulu, S. Ju, B. Kim, W.-T. Han, and C. Jayasankar, "Spectroscopic and pump power dependent up-conversion studies of Er^{3+}-doped lead phosphate glasses for photonic applications," *Journal of Alloys and Compounds*, vol. 699, pp. 959–968, 2017.

[16] M. M. Ismail, H. Farouk, M. A. Salem, A. Ashery, and I. K. Battisha, "Optical properties of Er^{3+} doped phosphate glasses," *Journal of Scientific Research in Science*, vol. 36, no. 1, pp. 469–483, 2019.

[17] Y. A. Lakshmi, K. Swapna, K. S. R. K. Reddy, M. Venkateswarlu, S. Mahamuda, and A. Rao, "Structural, optical and nir studies of Er^{3+} ions doped bismuth boro tellurite glasses for luminescence materials applications," *Journal of Luminescence*, vol. 211, pp. 39–47, 2019.

[18] J. Gomes, A. Lima, M. Sandrini, A. Medina, A. Steimacher, F. Pedrochi, and M. Barboza, "Optical and spectroscopic study of erbium doped calcium borotellurite glasses," *Optical materials*, vol. 66, pp. 211–219, 2017.

[19] K. Swapna, S. Mahamuda, M. Venkateswarlu, A. S. Rao, M. Jayasimhadri, S. Shakya, and G. V. Prakash, "Visible, up-conversion and nir (˜ 1.5 μm) luminescence studies of Er^{3+} doped zinc alumino bismuth borate glasses," *Journal of Luminescence*, vol. 163, pp. 55–63, 2015.

[20] A. Saeed, S. Sobaih, W. Abu-raia, A. Abdelghany, and S. Heikal, "Novel Er^{3+} doped heavy metals-oxyfluorophosphate glass as a blue emitter," *Optical and Quantum Electronics*, vol. 53, no. 8, p. 482, 2021.

[21] M. Graça, M. Ferreira da Silva, and M. A. Valente, "Structural and electrical properties of sio2–li2o–nb2o5 glass and glass–ceramics obtained by thermoelectric treatments," *Journal of Materials Science - J MATER SCI*, vol. 42, pp. 2543–2550, 04 2007.